Fukushima J. Med. Sci.,
Vol. 62, No. 1, 2016

[Original Article]

Radiation survey on Fukushima Medical University premises about four years after the Fukushima nuclear disaster

Yasutaka Omori[1)], Hiroaki Wakamatsu[2)], Atsuyuki Sorimachi[1)] and Tetsuo Ishikawa[1)]

[1)]Department of Radiation Physics and Chemistry, [2)]Student in School of Medicine, Fukushima Medical University, Fukushima, Japan

(Received May 22, 2015, accepted December 3, 2015)

Abstract

This study was conducted on the Fukushima Medical University (FMU) premises (in Fukushima City, Fukushima Prefecture) about four years after the Fukushima Daiichi Nuclear Power Plant accident. Its objectives were (1) to create a map of the ambient gamma dose rate (air-kerma rate) distribution, (2) to evaluate the air-kerma rate originating from natural radionuclides, and (3) to investigate the effects of snow cover on changes in the air-kerma rate. This man-borne survey revealed that the air-kerma rate varies widely, ranging from 0.038 μGy h^{-1} to 0.520 μGy h^{-1}, and is higher on grass than on the other investigated surface types, such as soil, asphalt, and bricks. In this area, the mean air-kerma rate from natural radiation was evaluated to be 0.03 ± 0.01 μGy h^{-1}, which is close to 0.04 μGy h^{-1}, which was measured in central Fukushima City by a local authority. Furthermore, snowfall was found to reduce the air-kerma rate by 5%-30%. This reduction was attributed to attenuation of the primary radiation while passing through the snow cover, and the measured contribution of scattered radiation to the air-kerma rate reduction was small. The reduction rate was found to depend on the initial snow depth but to maintain a similar value for a couple of days, after the snow had partially melted and its depth had decreased. Finally, analysis of the daily dose due to external exposure received on the FMU premises revealed that no further health effects due to chronic radiation exposure at this site are to be expected.

Key words : Air-kerma rate, Cesium, Fukushima nuclear disaster, Natural radionuclides, Snow cover

Introduction

Large amounts of artificial radionuclides released due to the Fukushima Daiichi Nuclear Power Plant (FDNPP) accident were deposited on the ground, mainly in the eastern and central parts of Fukushima Prefecture[1-3)]. On March 15, 2011, contaminated air masses flowed northwestward from FDNPP, and the artificial radionuclides were deposited along with rainfall in Fukushima City, the capital city of Fukushima Prefecture[4,5)]. Fukushima Medical University (FMU ; 37.69°N, 140.47°E, 180 m in altitude) is located at about 7 km south of central Fukushima City (70 m in altitude) and about 60 km northwest of FDNPP (Fig. 1). The university organized a team who conducted radiation measurements on the university premises about one month after the nuclear disaster[6,7)]. These surveys were repeated twice a month for the first year, once a month for the second year, and every two months for the third year, and currently, they are repeated every three months, though fewer points are measured than those in the previous surveys[8)].

The radiation survey conducted in this study was designed for three purposes. The first was to create a map showing the spatial distribution of the

Corresponding author : Yasutaka Omori E-mail : ys-omori@fmu.ac.jp
https://www.jstage.jst.go.jp/browse/fms http://www.fmu.ac.jp/home/lib/F-igaku/

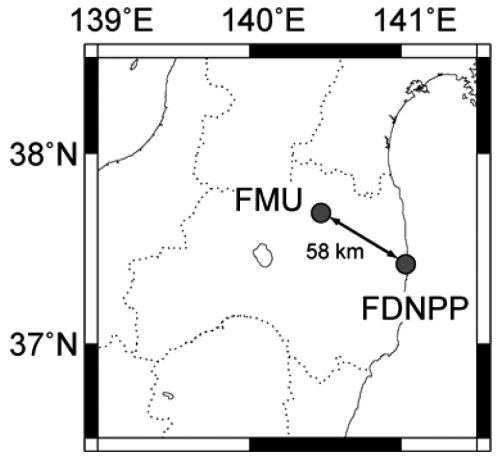

Fig. 1. Locations of FMU and FDNPP in Fukushima Prefecture, Japan. This figure was drawn using Generic Mapping Tools[49].

ambient gamma dose rate. As demonstrated by Bossew[9], ambient gamma dose rates have heterogeneous distributions even on a small horizontal scale (～20 m). In addition, it has been reported that the apparent half-lives of deposited radionuclides depend on the surface properties and land use[7,10], implying that artificial radionuclides can migrate and be redistributed. Both the magnitudes and spatial distributions of ambient gamma dose rates are variable with time, and, therefore, creating and updating dose rate distribution maps can facilitate radiation protection and decontamination.

The second purpose of this study was to investigate terrestrial radiation from natural radionuclides, which include elements of ^{238}U and ^{232}Th series and ^{40}K and contribute to about 20% of the globally averaged annual effective dose (excluding medical exposure)[11]. The gamma dose rate from natural radionuclides depends on the local geology of the measurement site[12,13]. At FMU, the gamma dose rate was only measured indoors, by using a thermoluminescence dose meter[14] ; the outdoor dose rate has not been reported yet.

The final purpose of this study was to examine the effects of snow cover on the ambient gamma dose rate from artificial radionuclides. In the winter, snowfall sometimes occurs in Fukushima Prefecture, and it is believed to affect the gamma dose rate, which has been reported to decrease with snow cover[15-17]. Sievert and Hultqvist[15] were the first to construct a model of snow cover shielding of natural radiation. This model related the reduction rate to snow depth and snow density. Their model was updated by Fujimoto[18], who modified the ratio of the contributions of primary and scattered radiation. Nagaoka *et al*.[19] presented a calculation method, which differed from the model of Fujimoto[18] by only a few percent, that yielded results in close agreement with the observational results. They also showed that the model was applicable even in non-ideal conditions (e.g., on a gentle slope or under an inhomogeneous distribution of snow accumulation due to partial snow removal). However, the ambient gamma dose rate reduction was not examined in case of lower-density snow (e.g., 0.1 g cm^{-3} (fresh snow)). In addition, these studies did not focus on radiation from artificial radionuclides.

In this study, we conducted a man-borne survey of the ambient gamma dose rate (air-kerma rate) to create a map of its spatial distribution on the FMU premises in the winter of 2015. At several measurement points, gamma ray pulse-height distributions were obtained to evaluate the contributions of natural and artificial radionuclides to the air-kerma rate. In addition, some snowfall events occurred during the months in which the survey was conducted. During these events, the air-kerma rate reduction due to the snow cover was analyzed.

Finally, the doses due to external exposure received on the FMU premises were estimated and found to be comparable to the globally obtained dose due to natural radiation ; hence, no additional health effects due to chronic exposure to radiation from the deposited artificial radionuclides are expected.

Materials and methods

Site characteristics

The FMU premises contain lecture and research buildings for medicine and nursing ; a university hospital ; an auditorium ; a library ; a gymnasium ; fields for baseball, tennis, archery, and soccer ; yards with grass, moss, and trees ; and parking areas (Fig. 2). Some of them were reconstructed or newly established after the nuclear disaster. In chronological order, four primary developments on the FMU premises are as follows : (1) the westernmost part of the parking area near the nursing building, which was destroyed by the 2011 Tohoku-Oki earthquake, was reconstructed and repaved with asphalt in April 2011 ; (2) the soccer field and nearby parking area were established on a former athletic field in March 2014 ; (3) a parking area was developed by cutting down a hill on the west side of the tennis court in September 2014 ; (4) some buildings are being constructed in former parking areas around the university hospital since July 2014 (the latter two parking area and construction sites

Fig. 2. Aerial photo of FMU (dated April 2, 2014). Symbols represent medical buildings (1), nursing building (2), university hospital (3), auditorium (4), library (5), gymnasium (6), baseball field (7), tennis court (8), archery field (9), soccer field (10), yards (Y), parking areas (P), and monitoring post for radiation measurement (M). Scale bar length is equivalent to 200 m.

((3) and (4)) are not pictured in Fig. 2).

Before this study was conducted, decontamination was officially performed in several areas. Sludge was removed from the gutters (including rain water drains) near the gymnasium, tennis court, and parking area in front of the nursing building, and they were pressure-washed. The top 5 cm of topsoil was removed from a 3,170 m^2 area on the archery field, and it was then buried 50 cm under vacant lots on the west and east sides of the field. Although topsoil was also removed from a 13 m^2 area behind the third-base dugout of the baseball field, decontamination has not been performed in the infield or outfield, and, therefore, the decontaminated area is much smaller than the area that has not been decontaminated. These procedures were conducted in 2011. In 2014, the rooftops of most buildings and a parking area near the gymnasium were decontaminated.

Man-borne survey of air-kerma rate

A man-borne survey of the air-kerma rate was conducted on sunny and cloudy days from January 20 to February 25, 2015. The survey was performed outdoors at 1 m above the ground level on the playfields, yards, and parking areas and along the roads and paths between the buildings. For the survey, a CsI(Tl) scintillation survey meter (PDR-111, Hitachi-Aloka Medical Ltd., Japan) was used, for which a calibration factor of 0.98 was obtained in a calibration test using a ^{137}Cs source in June 2013. According to the survey meter manual[20], its measurements deviate from the actual values by less than 15%. Each measurement lasted a few to several minutes, depending on the air-kerma rate. At each point, four measurements were made in different directions.

The employed survey meter displays values in units of μSv h^{-1}. In addition, its response to 0.06-1.25 MeV gamma rays varies by a factor of 0.5-2.0 (reference : ^{137}Cs)[20]. In this study, the measured values were compared to the air-kerma rates estimated from gamma ray pulse-height distribution measurements in order to obtain a conversion factor. The measurements (n = 19) were performed by using a spectrometer held 1 m above ground level over various surface types (soil/gravelly soil/grass/artificial turf) in the presence or absence of snow cover. The details of the measurement method and the analysis of the pulse-height distributions used to

calculate the air-kerma rates are described in the next section. A positive linear correlation was found between the measured values and air-kerma rates, and the conversion factor was found to be 0.642 Gy Sv^{-1} (standard error : 0.013 Gy Sv^{-1}, Fig. 3). This conversion factor is in agreement with the values of 0.623 Gy Sv^{-1} and 0.640–0.652 Gy Sv^{-1} that were obtained previously in the Tohoku region[21] and in an uncontaminated area in Aomori Prefecture[22], respectively, using the same survey meter. Consequently, the effect of the energy response of the survey meter on the measured values was considered to be small, and only one conversion factor was applied to calculate the air-kerma rates.

To draw the air-kerma rate distribution map, the geographic coordinates at each measurement point were recorded by a handheld GPS (eTrex 30J, Garmin Ltd., Switzerland), and the air-kerma rates were then plotted using Google Earth.

Estimation of natural and artificial radiation

To measure the radiation from the artificial and natural radionuclides separately, the pulse-height distributions of the incident gamma rays were obtained and analyzed. In this study, a 3 in × 3 in NaI(Tl) scintillation spectrometer (EMF-211, EMF Japan Co. Ltd., Japan) was used. The detector of the spectrometer was directed horizontally at 1 m above the ground, and each measurement lasted 900 s. The pulse-height distributions were unfolded in energies of 0.05–3.2 MeV (energy bin widths : 0.10–0.28 MeV) based on a 22 × 22 response matrix method typically used to obtain incident gamma-ray flux density energy spectra[23–25]. In this analysis, overlapping of the 1.365 MeV ^{134}Cs photon peak to the 1.464 MeV ^{40}K photon peak was removed[25].

The air-kerma rates from natural and artificial radiation were calculated based on the energy and flux densities of the incident gamma rays, the mass energy-absorption coefficient for air, and the dose conversion factors corresponding to each of the 22 energy bins[23,24]. Here, although the absorbed dose rate in air was the quantity actually calculated, it can be practically regarded as the air-kerma rate for environmental gamma radiation. To determine the air-kerma rates from natural radiation, we focused on the energy bins including the photon peaks of ^{40}K (1.464 MeV), ^{214}Bi (1.765 MeV and 2.205 MeV, ^{238}U-series element), and ^{208}Tl (2.615 MeV, ^{232}Th-series element). The concentrations of ^{40}K, ^{238}U, and ^{232}Th were calculated by comparing the observed energy spectra with those simulated using unit concentrations of these elements in the soil. Then, applying dose conversion factors to account for the concentrations of the respective elements, the air-kerma rates were calculated. The air-kerma rates

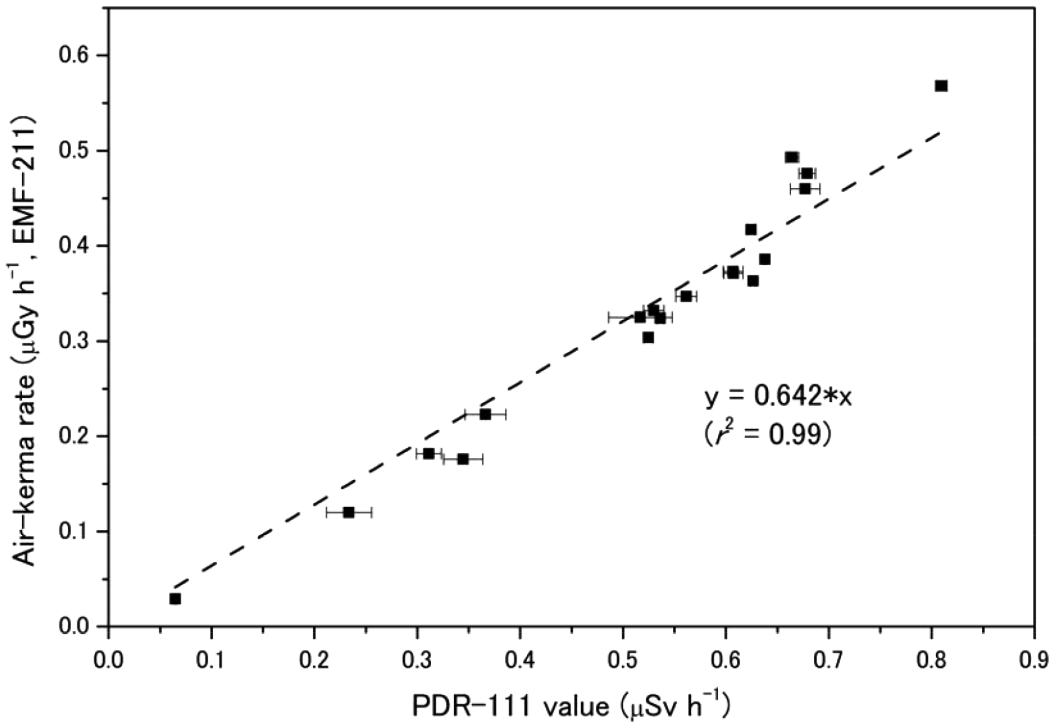

Fig. 3. Scatter plots of air-kerma rates against measured PDR-111 values. Data were obtained in presence (n = 13) and absence (n = 6) of snow cover. Bars represent standard deviations calculated from four measurements at each point. Broken line was fitted assuming intercept of zero.

for ^{134}Cs and ^{137}Cs were determined based on the gamma-ray flux density distributions in the 0.05-0.85 MeV energy bins, excluding the contributions from natural radiation. In the analysis, the flux densities in the 0.05-0.45 MeV energy bins were assumed to result from scattered radiation, while those in the 0.45-0.85 MeV energy bins were considered to be due to both primary and scattered radiation. Linear interpolation was performed in the flux densities to determine those caused by scattered radiation, and the remaining densities were regarded as resulting from primary radiation. The details of this analysis method are described by Yoshida *et al*.[26].

The measurement points were selected carefully because the response matrix method can only be applied to infinite-plane radiocesium sources on the ground and homogenous natural radionuclide distributions in the soil. Two points were selected on the baseball field, three in the yards, and one in the newly developed parking area near the tennis court ; the surfaces of all of these areas are unpaved.

Measurements during and after snowfall

During this study, snowfalls were observed by Japan Meteorological Agency in center of Fukushima City, on January 15, 17-18, and 30, as well as on February 13-15 and 18, 2015[27]. For the snowfalls on January 17-18 and February 13-15, snow cover had hardly been seen on the FMU premises when the radiation measurements began. Thus, the snowfalls on January 15 and 30 and February 18 were defined as the first, second, and third snowfall events, respectively. During the three snowfall events, using the same method as in the man-borne survey, the air-kerma rates were measured in the yards, tennis court, and baseball field by the survey meter, and the snow depth at each location was also determined. During the first and second events, the spectrometer was also used. During the third event, the bulk snow densities on the tennis court and baseball field were determined by measuring the weight of snow that was collected in a plastic cup (55.4 cm^3) from a cross-section of accumulated snow. The air-kerma rates were compared in the presence and absence of snow cover.

Estimation of dose due to external exposure received on FMU premises

Based on the air-kerma rate measurements, the doses due to external exposure on the FMU premises were estimated. We assumed two typical university life cases : (1) a university student spending 8 h in buildings for lectures and 3 h on the baseball field for a club activity and (2) a student spending 11 h only in buildings. Here, the baseball field was chosen due to higher air-kerma rates in that area (see the next section). The air-kerma rate in the buildings was set to that in our second-floor laboratory in building #4. The air-kerma rate was daily performed (n = 19) during this survey by using the survey meter.

Different conversion factors from air-kerma rate to effective dose rate are given for exposures to natural and artificial radiation. According to Moriuchi *et al*.[28], the conversion factor is 0.748 Sv Gy^{-1} for exposure to natural radiation. In contrast, the conversion factor for exposure to artificial radiation (^{134}Cs and ^{137}Cs) was calculated to be 0.73 Sv Gy^{-1}, considering the conversion factors from ambient dose equivalent rate to effective dose rate (0.58 Sv Sv^{-1} for ^{134}Cs and 0.57 Sv Sv^{-1} for ^{137}Cs)[29] and the ratio of ambient dose equivalent rate to air-kerma rate (1.25 Sv Gy^{-1})[30]. For the more conservative dose estimation, the conversion factor of 0.748 Sv Gy^{-1} was used.

Results

Spatial distribution of air-kerma rate

Fig. 4 shows the spatial distribution of the outdoor air-kerma rates on the FMU premises. The total number of measurement points was 136, consisting of points in the yards (n = 21), playfields (n = 15), parking areas (n = 57), and roads and paths (n = 43). About half of the surfaces were covered with asphalt. The air-kerma rates vary widely from 0.038 μGy h^{-1} to 0.520 μGy h^{-1}, with an arithmetic mean of 0.175 ± 0.108 μGy h^{-1} (see also Appendix). Higher values were measured in the yards and playfields. The maximum value was obtained on the grass in the baseball field, although more moderate values were obtained on the soil in the same field. In contrast, lower air-kerma rates were measured in the parking areas, roads, and paths. In particular, the lowest value was obtained in the parking area in the westernmost part of the FMU premises, which was developed after the nuclear disaster (see the above descriptions of the site characteristics). In Fig. 5, the frequency distribution of the air-kerma rates is shown. At more than half of the measurement points, the air-kerma rates are less than 0.15 μGy h^{-1} (the maximum air-kerma rate from terrestrial gamma radiation obtained by nationwide surveys in Japan[12]).

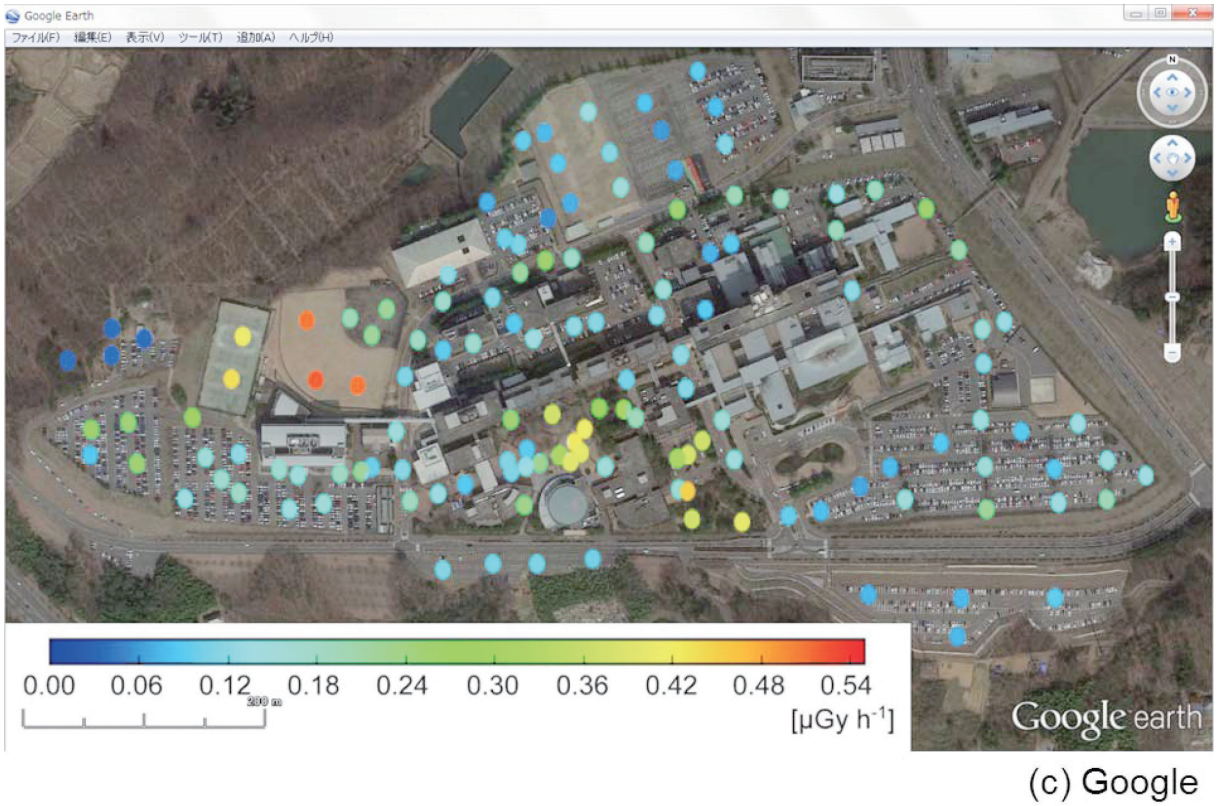

Fig. 4. Spatial distribution of air-kerma rates on FMU premises (n = 136). Scale bar length is equivalent to 200 m.

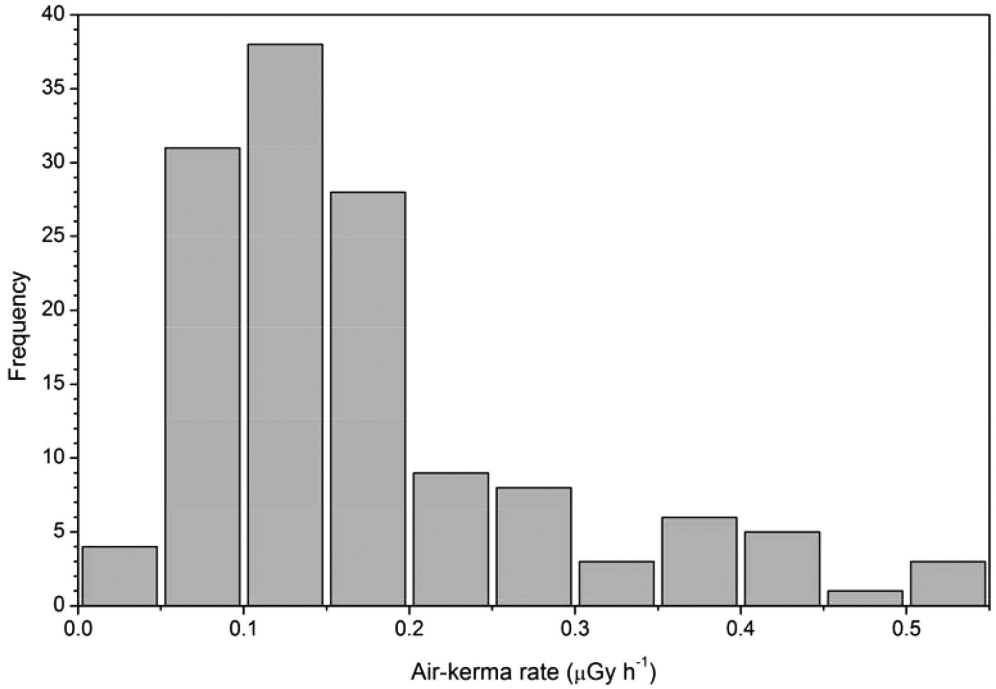

Fig. 5. Frequency distribution of air-kerma rates (n = 136).

Fig. 6 presents scatter plots of the relative standard deviations versus the air-kerma rates. The highest relative standard deviation was obtained near plants on the road.

Fig. 7 displays the air-kerma rates on five types of ground surfaces : asphalt (n = 76), bricks (including stone pavement, n = 18), soil/gravelly soil (n = 13), artificial turf (n = 2), and grass (n = 8)

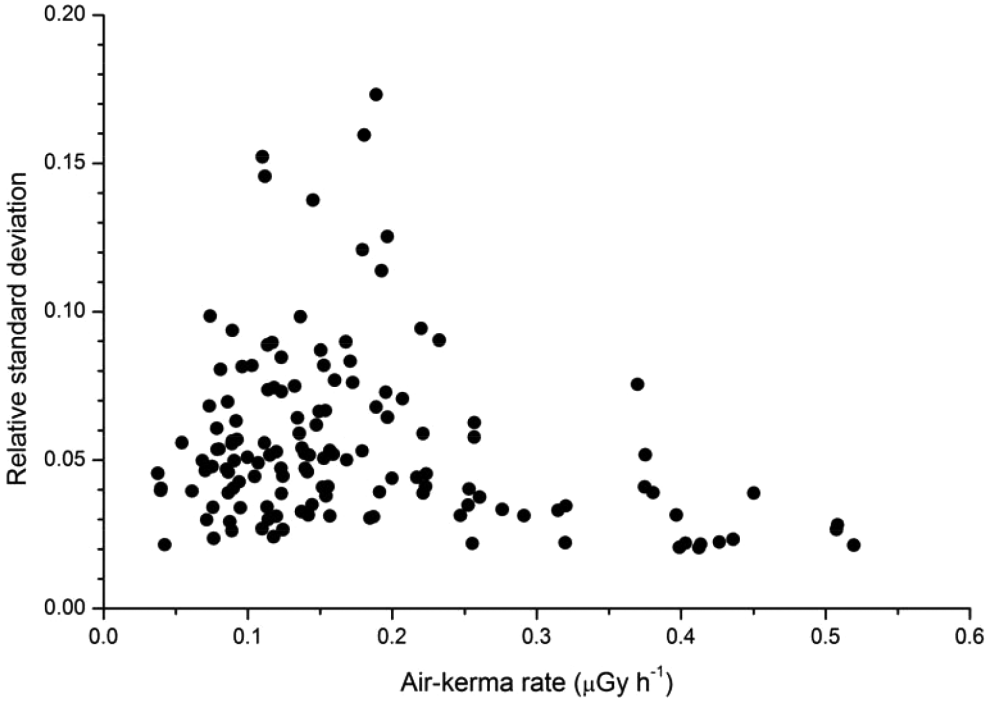

Fig. 6. Scatter plots of relative standard deviation against air-kerma rate.

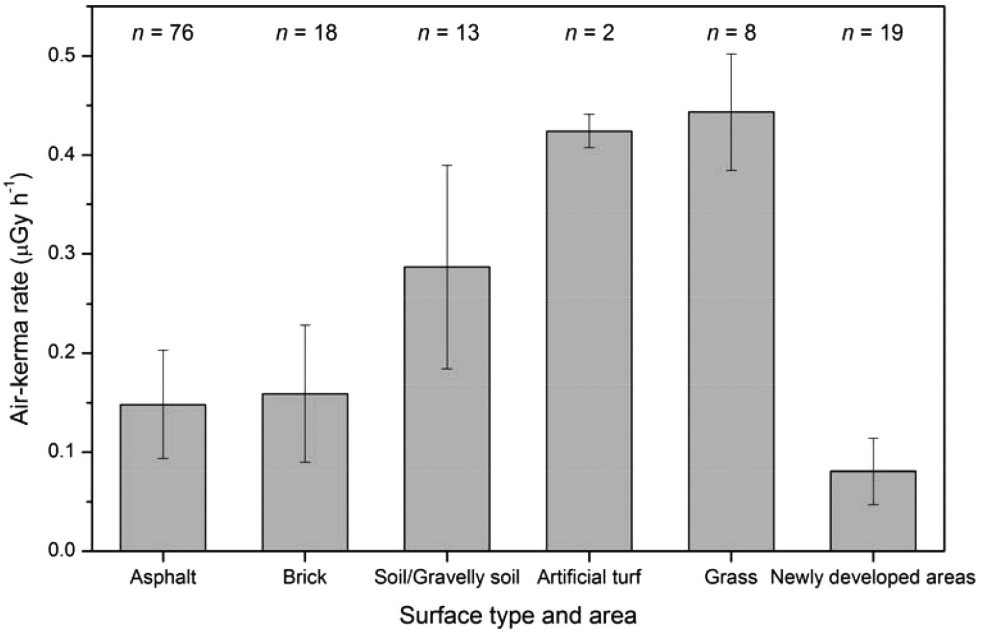

Fig. 7. Air-kerma rates on different surface types and in newly developed areas. Vertical bars represent standard errors.

and in newly developed areas (n = 19). It is evident that the air-kerma rates on the different surface types vary significantly. They are lower on asphalt and bricks than on soil and grass. However, the newly developed areas clearly exhibit the lowest air-kerma rates, although various surface types (asphalt, soil, gravelly soil, and grass) exist in these areas.

Contributions of natural and artificial radionuclides to air-kerma rate

The air-kerma rates from natural and artificial radionuclides were evaluated by applying the response matrix method to the gamma ray pulse-height distributions obtained with the spectrometer. The contributions of artificial radionuclides, except

for those of ^{134}Cs and ^{137}Cs, were not identifiable in the pulse-height distributions (data not shown). Table 1 presents the air-kerma rates from natural, artificial and all radionuclides in the yards, baseball field, and unpaved parking area. As shown, the air-kerma rate from artificial radionuclides constitutes 50%–90% of the total rate. The air-kerma rate from natural radionuclides is 0.029 ± 0.008 μGy h^{-1}, with a range of 0.013–0.035 μGy h^{-1}, and is nearly constant regardless of the surface type, except in the parking area. According to Minato[31], terrestrial gamma radiation originates from the top 30 cm of soil. Since the parking area was developed by cutting down a hill by several meters, the topsoil in that area may be different from that in the other areas, causing the observed difference in the air-kerma rate.

Air-kerma rate reduction due to snow cover

Fig. 8 shows the temporal air-kerma rate

Table 1. Air-kerma rates from artificial and natural radionuclides.

Location	Date (YYYY/MM/DD)	Air-kerma rate (μGy h^{-1})[1]		
		Total	^{134}Cs + ^{137}Cs	Natural
Yard (grass)	2015/01/23	0.493	0.457	0.035
Yard (trees)	2015/02/25	0.291	0.261	0.030
Yard (moss)	2015/02/25	0.468	0.437	0.031
Baseball field (soil)	2015/01/28	0.176	0.146	0.030
Baseball field (grass)	2015/01/28	0.568	0.534	0.034
Parking (unpaved)	2015/03/30	0.029	0.016	0.013
Average				0.029
Standard error				0.008

[1] One measurement was made at each location.

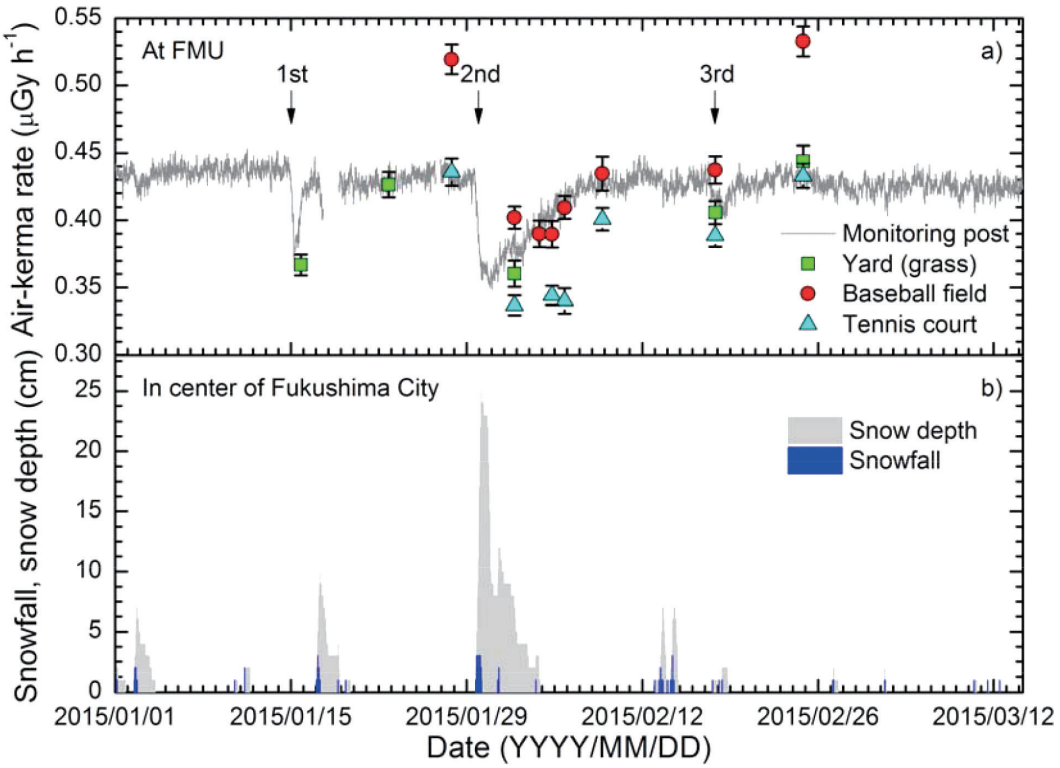

Fig. 8. Time-series variations of air-kerma rates on FMU premises obtained from spot measurements with survey meter and continuous measurement (sampled every 10 min ; 7-point moving average) with monitoring post installed by Nuclear Regulation Authority[32]. Vertical bars represent one standard deviation. Arrows indicate snowfall events examined in present study. Snowfall and snow depth were observed in center of Fukushima City by Japan Meteorological Agency[27].

variations on the FMU premises. One plot was constructed based on continuous measurements taken by a monitoring post (Fig. 2) installed by the Nuclear Regulation Authority[32], and the others were obtained from the survey meter spot measurements taken in the yard (on grass), baseball field (on grass), and tennis court (on artificial turf). Air-kerma rate reductions are clearly evident in the continuous measurements as well as in the spot measurements after the snowfall events and were estimated to be 5%–30%. During the second event, the duration of radiation reduction appears to differ between the two types of measurements. In the continuous measurements, recovery to the normal level began within a day after the air-kerma rate reached its minimum due to the presence of snow cover. In contrast, in the spot measurements, the radiation reduction continued for at least four days. This inconsistency may be due to the difference between the locations at which the two types of measurements were performed. At the continuous measurement location, there is a parking area for guests and vendors, and, therefore, snow removal was performed after the snowfall. In contrast, on the tennis court and baseball field, the snow was not removed artificially. This difference may have caused the radiation reduction durations to differ. In order to confirm this possibility, further investigations are necessary.

In this study, the dependence of the radiation reduction magnitude on the amount of snow cover was also investigated. For this analysis, the ratio of the converted air-kerma rate above the snow cover surface to a reference air-kerma rate calculated from the two values measured with the survey meter on January 23 (or 28) and February 25 (see Fig. 8) was introduced. The snow depths were 6 cm, 11–14 cm, and 4–8 cm on the FMU premises for the first, second, and third events, respectively. In addition, after the snowfall became light during the third event, the snow density was measured in the upper part of the snow cover, which consisted of fresher snow, as the lower part contained several-millimeter-thick ice. The density was found to be 0.15 $\pm$ 0.03 g cm^{-3} (0.11–0.19 g cm^{-3}; n = 4) at both the baseball field and the tennis court. Fig. 9 shows scatter plots of air-kerma rate ratio versus snow depth. It is clear that the air-kerma rate ratio decreases with increasing snow depth. With the deepest snow cover (in the second event), it decreases by about 30%, while with the shallowest snow cover (in the third event), it is 5%–10%.

Gamma radiation can be divided into the primary and scattered radiation. For clarifying which type of radiation contributed to the reduction of the air-kerma rate when snow cover was present, the pulse-height distributions obtained using the spectrometer were analyzed. In this analysis, only the gamma rays emitted from ^{134}Cs and ^{137}Cs were focused on because the contribution of natural

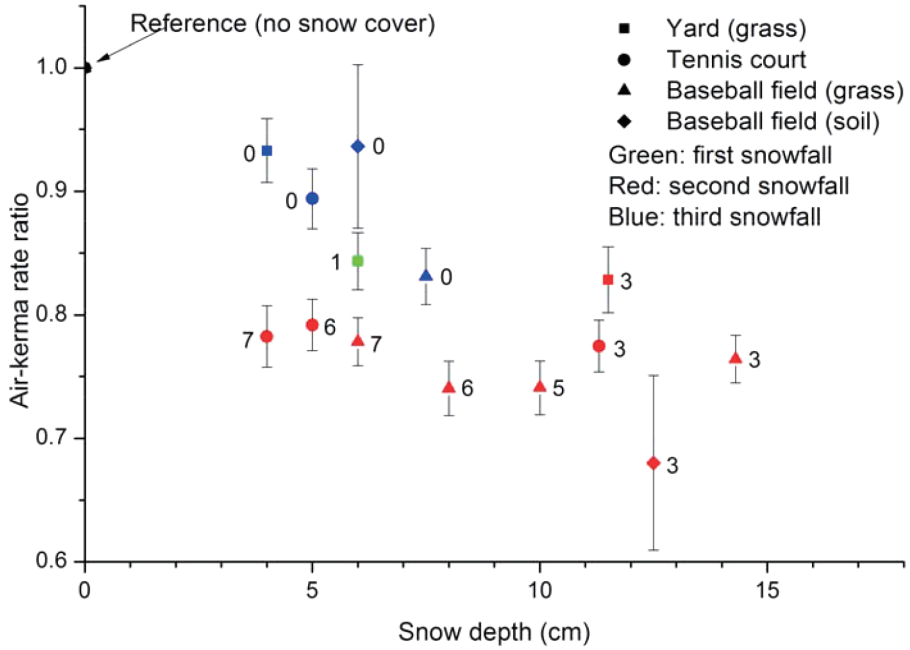

Fig. 9. Scatter plots of air-kerma rate ratio in presence and absence of snow cover. Ratio is unity with no snow cover. Reference value was calculated from two air-kerma rates obtained on separate days. Vertical bars were evaluated based on error propagation. Suffix numbers represent lapsed days after snowfall.

radionuclides to the air-kerma rate was very low compared to that of artificial radionuclides (Table 1). Fig. 10 shows the air-kerma rate ratios for primary and scattered radiation from ^{134}Cs and ^{137}Cs with respect to snow depth at five locations. Significant differences between the primary and scattered radiation air-kerma rate reductions are evident. The air-kerma rates from primary radiation decrease by 40%–50%, while those from scattered radiation decreases by at most 10%.

Daily dose received on FMU premises

The arithmetic mean of air-kerma rate in our laboratory was 0.034 ± 0.001 μGy h^{-1} (n = 19). The contributions of ^{134}Cs and ^{137}Cs were not included in this value since the photon peaks of these isotopes were hardly identifiable in the gamma ray pulse-height distribution (measurement time : 900 s) obtained in the laboratory by using the spectrometer (data not shown). In addition, the arithmetic mean of the air-kerma rate on the baseball field was calculated to be 0.363 μGy h^{-1}. Consequently, effective doses over 11 h in the first and second university life cases were estimated to be 1.0 μSv and 0.3 μSv, respectively.

Discussion

One month after the nuclear disaster, the air-kerma rates were observed to be 0.66–2.54 μGy h^{-1} (ambient dose equivalent rates : 0.82–3.18 μSv h^{-1}) on the FMU premises[6,8]. In this study, it was determined that they had decreased to 0.04–0.52 μGy h^{-1} about four years later. The rapid decreases in the air-kerma rates are considered to be governed not only by the physical decays of ^{134}Cs (2.1 years), ^{137}Cs (30.0 years), and any other short-lived artificial radionuclides, but also by climate factors and human activities. The climate factors are considered to be wash-off by rainfall and resuspension by wind[33–36]. In addition, these factors are more effective on paved surfaces, resulting in lower radiocesium concentrations (and air-kerma rates) on paved surfaces than on unpaved surfaces[6,7,37,38]. In this study, the air-kerma rates were found to be higher on grass and soil than asphalt (Fig. 7). This characteristic is in agreement with the previous results. Kakamu *et al.*[7] also previously observed the same characteristic just one month after the nuclear disaster, however, subsequently, the apparent half-life was longer on asphalt than it was on soil or grass. Assuming that the air-kerma rate distribution was homogeneous upon the initial deposition of radiocesium, this result may imply that the adherence rate was low but the adhered radiocesium was not easily removed from the asphalt on the FMU premises. On the soccer

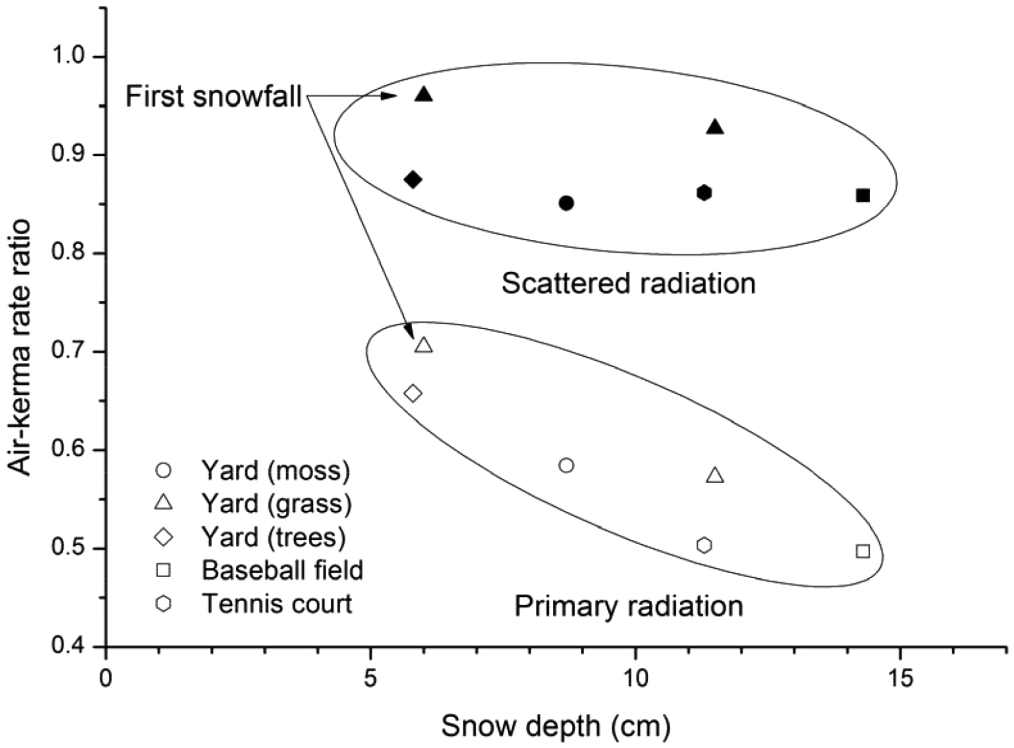

Fig. 10. Air-kerma rate reductions due to snow cover for primary and scattered radiation from deposited radiocesium. Data were obtained in first and second snowfall events.

field and parking areas in the northernmost part of the FMU premises, the air-kerma rates of 2.18–2.54 μGy h^{-1} (ambient dose equivalent rates : 2.72–3.18 μSv h^{-1}) on April 11, 2011 (noted as a track field in Tsuji *et al.*[6]) decreased to 0.06–0.16 μGy h^{-1}. These areas were developed after the nuclear disaster, which probably caused the significant decreases in the air-kerma rates.

In this study, the air-kerma rates from natural radionuclides on the FMU premises were observed to be 0.01–0.04 μGy h^{-1}. According to earlier reports[39,40], air-kerma rates of 0.02–0.07 μGy h^{-1} (0.04 μGy h^{-1} in Fukushima City) were measured by a survey meter in Fukushima Prefecture before the nuclear disaster. In addition, in a health management survey for Fukushima inhabitants, an air-kerma rate of 0.04 μGy h^{-1} from natural radionuclides was considered to evaluate additional external exposure during the four months following the nuclear disaster[29,41]. The results of this study are comparable to those of the previous studies.

The results of this study demonstrate that air-kerma rates are reduced with snow cover and are reduced more with greater snow depths. However, snow depth alone does not govern radiation reduction. In fact, the air-kerma rates during the second and third snowfall events differed even when the snow depths were the same (Fig. 9). In addition, a longer radiation reduction duration was observed even when the snow cover decreased during the second event (Figs. 8 and 9). These differences may have been caused by dissimilar snow densities on the measurement dates. During the third event, fresh snow accumulated on the measurement date and had a density of about 0.15 g cm^{-3}. This value was obtained by a simple method, but it was confirmed by another evaluation based on the amounts of rainfall (1.5 mm, an equivalent value) and snowfall (1 cm) measured by the Japan Meteorological Agency in the center of Fukushima City[27]. In contrast, during the second event, the first measurement was made three days after the snowfall (Fig. 8). According to the meteorological data provided by the Japan Meteorological Agency[27], the snow had a density of 0.09 g cm^{-3} (an estimated value), its depth reached 25 cm on January 30 (intermittent accumulation (4 cm) occurred on February 1), and its depth then decreased to 8 cm by February 2 (Fig. 8b). It can be presumed that the snow density increased as the snow cover melted. This hypothesis is supported by a study by Kondo and Numata[42], who reported that snow density can increase from 0.1 g cm^{-3} to 0.25 g cm^{-3} within a few days after it falls. Thus, the snow density, which increased as the snow melted, possibly caused the air-kerma rate decrease to be greater than that for fresh snow even with the same snow depth. These findings are in agreement with those of the terrestrial gamma radiation studies by Fujimoto[18] and Nagaoka *et al.*[19], who noted that the water equivalent ([snow depth]×[snow density]) is a key parameter in evaluating radiation reduction. Based on these studies, the longer radiation reduction duration shown in Figs. 8 and 9 indicates that the water equivalent was conserved and, therefore, the reduction efficiency was constant throughout the measurement period. In order to clarify the dependence of artificial radiation reduction on snow cover, further investigations including simultaneous measurements of snow depth and snow density are necessary. In addition, in the present study, the bulk density of the snow was measured, excluding the thin layer of ice underneath the snow. However, unlike on the FMU premises, in heavy snowfall areas, the vertical snow density distribution can vary from 0.1 g cm^{-3} to 0.6 g cm^{-3} from the upper part to the lower part and over time[43,44]. In such areas, the effects of the vertical density distribution on the radiation reduction cannot be ignored.

The results of this study also indicate that the radiation reduction due to snow cover is related to changes in the ratio between the air-kerma rate contributions from primary and scattered radiation (Fig. 10). That is, only primary radiation is significantly reduced with snow cover. Assuming that snow is equivalent to water in composition and that its effective atomic number is 7.5, Compton scattering mainly affects the primary radiation (0.6–0.8 MeV) that travels through the snow cover. Therefore, some of the primary radiation that interacts with the snow can be detected as scattered radiation. In contrast, the reduction of the scattered radiation from the deposited radiocesium due to snow cover appeared negligible. For lower-energy scattered radiation, photoelectric absorption has a greater effect than it does on primary radiation. In snow, absorption and generation by Compton scattering of the primary radiation occur simultaneously, so the air-kerma rate reduction for scattered radiation is considered to be small.

Effective doses received in two typical university life cases on the FMU premises were estimated to be 0.3–1.0 μSv. One month after the nuclear disaster, Tsuji *et al.*[6] estimated the effective dose of the university student to be 9.8 μSv over 10.3 h

(spending 7 h in buildings and 3.3 h on the athletic field and a parking area). At present it remarkably decreases by about 90% although the estimation conditions are slightly different between Tsuji *et al.*[6] and this study. Our estimated values include the contributions of natural radionuclides. Even if radiation exposure at these equivalent levels continues daily for an entire year, the received doses are within the globally obtained range of external exposure due to terrestrial radiation (0.3–1.0 mSv)[11].

Finally, based on the dose estimation, the possible health effects due to external exposure were determined based on epidemiological studies conducted in high-background-radiation areas worldwide. As mentioned previously, the air-kerma rates were 0.04–0.52 μGy h^{-1} on the FMU premises. These values are comparable to those in the high-background-radiation areas such as Kerala, India (0.04–2.1 μGy h^{-1}, outdoors)[45] and Yangjiang, China (0.26–0.60 μGy h^{-1}, indoors)[46]. The high air-kerma rates in these areas are attributed to the presence of naturally occurring thorium-rich soil, which is distributed in along the coast in Kerala[45] and is used as in building materials in Yangjiang[46]. Epidemiological surveys on the health effects due to external exposure in these areas indicated no statistically significant increase in mortality due to cancer or non-cancer diseases[47,48]. Thus, except for health effects resulting from initial exposure shortly after the nuclear disaster, no additional health effects due to chronic exposure to radiation from the deposited artificial radionuclides are expected.

Acknowledgements

The authors would like to thank Mr. Keiichi Anzai in the Facilities Division of FMU for providing detailed information about the decontamination and construction development conducted on the FMU premises. The air-kerma rate distribution map was created by using a program developed by Prof. Takanobu Ogawa of Seikei University. This paper was improved by valuable and constructive comments from two reviewers.

Conflicts of interest

The authors declare no conflicts of interest.

Appendix

The air-kerma rates obtained in the man-borne survey on the FMU premises are listed in Table A1.

Table A1. Air-kerma rates obtained in man-borne survey on FMU premises.

Location	Air-kerma rate (μGy h^{-1}) Mean±SD	Surface type
Yard-1 (Y1)	0.092±0.006	Brick
	0.113±0.004	Brick
	0.136±0.008	Brick
	0.223±0.010	Asphalt
	0.426±0.010	Grass
	0.320±0.007	Gravelly soil
	0.397±0.013	Grass
	0.399±0.008	Grass
	0.413±0.009	Grass
	0.375±0.015	Grass
	0.114±0.010	Brick
	0.253±0.010	Asphalt
	0.276±0.009	Gravelly soil with trees
	0.315±0.010	Gravelly soil with trees
	0.107±0.005	Brick
	0.196±0.014	Brick
	0.153±0.008	Brick
	0.232±0.021	Stone pavement
Yard-2 (Y2)	0.160±0.012	Soil
	0.381±0.015	Brick

Location	Air-kerma rate (μGy h^{-1}) Mean±SD	Surface type
Yard-2 (Y2)	0.320±0.011	Soil
	0.370±0.028	Soil
	0.450±0.018	Soil with moss and trees
	0.375±0.019	Soil with moss and trees
	0.403±0.009	Soil with moss and trees
Archery field	0.095±0.003	Soil/Grass
Baseball field	0.221±0.013	Soil
	0.200±0.009	Soil
	0.223±0.009	Soil
	0.508±0.014	Grass
	0.520±0.011	Grass
	0.508±0.014	Grass
Soccer field	0.118±0.003	Soil/Grass
	0.142±0.004	Soil/Grass
	0.078±0.005	Soil/Grass
	0.089±0.002	Soil/Grass
	0.072±0.002	Soil/Grass
	0.157±0.008	Soil/Grass
Tennis court	0.436±0.010	Artificial turf
	0.412±0.008	Artificial turf
Paths between buildings	0.086±0.003	Brick
	0.134±0.009	Brick
	0.089±0.005	Asphalt
	0.168±0.008	Brick
	0.090±0.005	Asphalt
	0.140±0.007	Asphalt
	0.124±0.006	Asphalt
	0.117±0.010	Asphalt
Roads	0.189±0.033	Asphalt
	0.120±0.004	Asphalt
	0.151±0.013	Asphalt
	0.112±0.016	Asphalt
	0.181±0.029	Asphalt
	0.173±0.013	Asphalt
	0.115±0.006	Asphalt
	0.217±0.010	Asphalt
	0.257±0.016	Asphalt
	0.179±0.022	Asphalt
	0.191±0.007	Asphalt
	0.153±0.013	Asphalt
	0.120±0.006	Asphalt
	0.123±0.005	Brick
	0.118±0.009	Brick
	0.159±0.008	Brick
	0.144±0.005	Brick
	0.255±0.006	Asphalt
	0.196±0.025	Asphalt
	0.089±0.005	Asphalt

Location	Air-kerma rate (μGy h^{-1})	Surface type
	Mean±SD	
Roads	0.074±0.007	Asphalt
	0.089±0.008	Asphalt
	0.189±0.013	Asphalt
	0.136±0.013	Asphalt
	0.187±0.006	Asphalt
	0.257±0.015	Asphalt
	0.207±0.015	Asphalt
	0.132±0.010	Asphalt
	0.154±0.006	Asphalt
	0.193±0.022	Asphalt
	0.123±0.009	Asphalt
Parking area (gymnasium, P1)	0.103±0.008	Asphalt
	0.110±0.017	Asphalt
	0.073±0.005	Gravelly soil
	0.054±0.003	Gravelly soil
	0.124±0.003	Asphalt
Parking area (north, P2)	0.085±0.004	Gravelly soil
	0.092±0.005	Gravelly soil
	0.080±0.004	Gravelly soil
	0.114±0.008	Gravelly soil
	0.070±0.003	Gravelly soil
	0.061±0.002	Gravelly soil
Parking area (east, P3)	0.123±0.010	Asphalt
	0.145±0.020	Asphalt
	0.087±0.003	Asphalt
	0.090±0.004	Asphalt
	0.137±0.004	Asphalt
	0.148±0.009	Asphalt
	0.197±0.013	Asphalt
	0.139±0.007	Asphalt
	0.137±0.007	Asphalt
	0.086±0.006	Asphalt
	0.157±0.005	Asphalt
	0.221±0.009	Asphalt
	0.152±0.006	Asphalt
	0.079±0.004	Asphalt
	0.069±0.003	Asphalt
	0.081±0.007	Asphalt
	0.096±0.008	Asphalt
Parking area (south east, P4)	0.076±0.002	Asphalt
	0.075±0.004	Asphalt
	0.094±0.004	Asphalt
	0.076±0.003	Asphalt
Parking area (south, P5)	0.105±0.005	Asphalt
	0.112±0.006	Asphalt
	0.110±0.003	Asphalt
	0.114±0.003	Asphalt

Location	Air-kerma rate (μGy h^{-1}) Mean±SD	Surface type
Parking area (west, P6)	0.100±0.005	Asphalt
	0.220±0.021	Brick
	0.184±0.006	Brick
	0.149±0.010	Asphalt
	0.168±0.015	Asphalt
	0.171±0.014	Asphalt
	0.155±0.006	Asphalt
	0.141±0.007	Asphalt
	0.179±0.010	Asphalt
	0.142±0.007	Asphalt
	0.154±0.010	Asphalt
	0.123±0.006	Asphalt
	0.291±0.009	Asphalt
	0.253±0.009	Asphalt
	0.247±0.008	Asphalt
	0.086±0.004	Asphalt
	0.260±0.010	Asphalt
	0.042±0.001	Gravelly soil
	0.040±0.002	Gravelly soil
	0.040±0.002	Gravelly soil
	0.038±0.002	Gravelly soil

References

1. Chino M, Nakayama H, Nagai H, Terada H, Katata G, Yamazawa H. Preliminary estimation of release amounts of ^{131}I and ^{137}Cs accidentally discharged from the Fukushima Daiichi Nuclear Power Plant into the atmosphere. J Nucl Sci Technol, **48** : 1129–1134, 2011.
2. Morino Y, Ohara T, Watanabe M, Hayashi S, Nishizawa M. Episode analysis of deposition of radiocesium from the Fukushima Daiichi Nuclear Power Plant accident. Environ Sci Technol, **47** : 2314–2322, 2013.
3. Torii T, Sugita T, Okada CE, Reed MS, Blumenthal DJ. Enhanced analysis methods to derive the spatial distribution of ^{131}I deposition on the ground by airborne surveys at an early stage after the Fukushima Daiichi Nuclear Power Plant accident. Health Phys, **105** : 192–200, 2013.
4. Kobayashi T. Radiation measurements at the campus of Fukushima Medical University through the 2011 off the Pacific coast of Tohoku earthquake and subsequent nuclear power plant crisis. Fukushima J Med Sci, **57** : 70–74, 2011.
5. Tsuruta H, Oura Y, Ebihara M, Ohara T, Nakajima T. First retrieval of hourly atmospheric radionuclides just after the Fukushima accident by analyzing filter-tapes of operational air pollution monitoring stations. Sci Rep, **4** : 6717, doi : 10.1038/srep06717, 2014.
6. Tsuji M, Kanda H, Kakamu T, *et al*. An assessment of radiation doses at an educational institution 57.8 km away from the Fukushima Daiichi nuclear power plant 1 month after the nuclear accident. Environ Health Prev Med, **17** : 124–130, 2012.
7. Kakamu T, Kanda H, Tsuji M, *et al*. Differences in rates of environmental radiation dose rates by ground surface property in Fukushima city after the Fukushima Daiichi nuclear power plant accident. Health Phys, **104** : 102–107, 2013.
8. Fukushima Medical University. Results of Environmental Radiation in Fukushima Medical University. Available at http://www.fmu.ac.jp/univ/chiiki/radiation.html, 2015 (accessed on May 16, 2015). (in Japanese)
9. Bossew P. Small-scale variability of the gamma dose rate in the urban environment of Fukushima city. Radiat Emerg Med, **2** : 64–68, 2013.
10. Kinase S, Takahashi T, Sato S, Sakamoto R, Saito K. Development of prediction models for radioactive caesium distribution within the 80-km radius of the Fukushima Daiichi nuclear power plant. Radiat Prot Dosim, **160** : 318–321, 2014.
11. United Nations Scientific Committee on the Effects of Atomic Radiation. Sources and Effects of Ionizing Radiation, UNSCEAR 2008 Report :

Volume I : Sources — Report to the General Assembly with Scientific Annexes A and B. United Nations, New York, 2010.
12. Furukawa M. Natural radiation level in Japan islands. J Geograph, **102** : 868–877, 1993. (in Japanese with English abstract)
13. Furukawa M, Shingaki R. Terrestrial gamma radiation dose rate in Japan estimated before the 2011 Great East Japan Earthquake. Radiat Emerg Med, **1** : 11–16, 2012.
14. Kobayashi T, Takaku Y. Comparisons of natural radiation at new and old campus of Fukushima Medical College. Jpn J Health Phys, **26** : 117–122, 1991. (in Japanese with English abstract)
15. Sievert RM, Hultqvist B. Variations in natural γ-radiation in Sweden. Acta Radiol, **37** : 388–398, 1952.
16. Iyogi T, Ueda S, Hisamatsu S, *et al*. Environmental gamma-ray dose rate in Aomori Prefecture, Japan. Health Phys, **82** : 521–526, 2002.
17. Yamazaki K, Tonouchi S, Hashimoto T. Factors associated with the variations in environmental gamma-ray spectra in Kashiwazaki Kariwa area. J Radioanal Nucl Chem, **252** : 359–366, 2002.
18. Fujimoto K. Shielding effect of snow cover on terrestrial gamma exposure rate. Jpn J Health Phys, **21** : 3–8, 1986. (in Japanese with English abstract)
19. Nagaoka T, Sakamoto R, Saito K, Tsutsumi M, Moriuchi S. Diminution of terrestrial gamma ray exposure rate due to snow cover. Jpn J Health Phys, **23** : 309–315, 1988. (in Japanese with English abstract)
20. Hitachi Aloka Medical Ltd. A Pocket Survey Meter MYRATE Model PDR-111 : a Manual. Hitachi Aloka Medical Ltd., Tokyo, 2015. (in Japanese)
21. Yoshino H, Obara H, Maeda T, *et al*. An investigation of gamma-ray dose rate in the central area of Hirosaki city, Japan. Radiat Emerg Med, **2** : 72–76, 2013.
22. Hosoda M, Fukui Y, Pornnumpa C, *et al*. Absorbed dose rate in air at the Bunkyo-cho campus of Hirosaki University. Radiat Emerg Med, **3** : 59–62, 2014.
23. Minato S. A response matrix of a 3″φ×3″ NaI(Tl) scintillator for environmental gamma radiation analysis. Rep Govern Indust Res Inst Nagoya, **27** : 384–397, 1978. (in Japanese)
24. Minato S. Diagonal elements fitting technique to improve response matrixes for environmental gamma ray spectrum unfolding. RADIOISOTOPES, **50** : 463–471, 2001.
25. Minato S. A method to discriminate natural radiation in cesium-bearing field based on a 22×22 response matrix method. Available at http://www1.s3.starcat.ne.jp/reslnote/CESIUM.pdf, 2012 (accessed on May 16, 2015). (in Japanese)
26. Yoshida HO, Hosoda M, Saito J, Kobayashi I, Hirasawa N. Effect of shieldings on ambient equivalent dose rate reduction inside resident's house after the Fukushima Daiichi nuclear power plant accident. RADIOISOTOPES, **62** : 203–210, 2013.
27. Japan Meteorological Agency. Past Meteorological Data. Available at http://www.data.jma.go.jp/obd/stats/etrn/index.php, 2015 (accessed on May 16, 2015). (in Japanese)
28. Moriuchi S, Tsutsumi M, Saito K. Examination on conversion factors to estimate effective dose equivalent from absorbed dose in air for natural gamma radiations. Jpn J Health Phys, **25** : 121–128, 1990. (in Japanese with English abstract)
29. Akahane K, Yonai S, Fukuda S, *et al*. NIRS external dose estimation system for Fukushima residents after the Fukushima Dai-ichi NPP accident. Sci Rep, **3** : 1670, doi : 10.1038/srep01670, 2013.
30. Saito K, Petoussi-Henss N. Ambient dose equivalent conversion coefficients for radionuclides exponentially distributed in the ground. J Nucl Sci Technol, **51** : 1274–1287, 2014.
31. Minato S. An Introduction to the Physics of Natural Environmental Radiation Fields. Government Industrial Research Institute, Nagoya, Japan, Nagoya, 1990.
32. Nuclear Regulation Authority. Monitoring Information of Environmental Radioactivity Level. Available at : http://radioactivity.nsr.go.jp/map/ja/, 2015 (accessed on May 16, 2015). (in Japanese)
33. Halldin S, Rodhe A, Bjurman B. Urban storm water transport and wash-off of caesium-137 after the Chernobyl accident. Water Air Soil Pollut, **49** : 139–158, 1990.
34. Mueck K, Steger F. Wash-off effects in urban areas. Radiat Prot Dosim, **37** : 189–194, 1991.
35. Garger EK, Kashpur V, Belov G, *et al*. Measurement of resuspended aerosol in the Chernobyl area. I. Discussion of instrumentation and estimation of measurement uncertainty. Radiat Environ Biophys, **36** : 139–148, 1997.
36. Garger EK, Kashpur V, Paretzke HG, Tschiersch J. Measurement of resuspended aerosol in the Chernobyl area. Part II. Size distribution of radioactive particles. Radiat Environ Biophys, **36** : 275–283, 1997.
37. Hosoda M, Tokonami S, Sorimachi A, *et al*. The time variation of dose rate artificially increased by the Fukushima nuclear crisis. Sci Rep, **1** : 87, doi10.1038/srep00087, 2011.
38. Kinase S, Sato S, Sakamoto R, Yamamoto H, Saito K. Changes in ambient dose equivalent rates around roads at Kawamata town after the

Fukushima accident. Radiat Prot Dosim, **167** : 340–343, 2015.
39. Fukushima Prefectural Atomic Energy Center. Report of Field Surveys on Natural Radioactivity (the Year 1995). Fukushima Prefectural Atomic Energy Center, Fukshima, 1996. (in Japanese)
40. Fukushima Prefectural Atomic Energy Center. Report of Field Surveys on Natural Radioactivity (the Year 1997). Fukushima Prefectural Atomic Energy Center, Fukshima, 1998. (in Japanese)
41. Ishikawa T, Yasumura S, Ozasa K, *et al*. The Fukushima Health Management Survey : estimation of external doses to residents in Fukushima Prefecture. Sci Rep, **5** : 12712, doi10.1038/srep12712, 2015.
42. Kondo J, Numata Y. Parameterization of the snow density in the top snow layer. J Jpn Soc Snow Ice (SEPPYO), **50** : 80–86, 1988. (in Japanese with English abstract)
43. Kojima K, Wakahama G, Nakamura N, *et al*. Report of snow cover observations, Sapporo, 1964–1965. Low Temp Sci Ser A, **24** : 159–174, 1967. (in Japanese with English abstract)
44. Ichiyanagi J, Gotoh K. Studies on the vertical distribution and time course changes of water quality in snowpack. Proc of Environ Engin Res, **30** : 81–89, 1993. (in Japanese with English abstract).
45. Hosoda M, Tokonami S, Omori Y, *et al*. Estimation of external dose by car-borne survey in Kerala, India. PLoS ONE, **10** : e0124433, doi : 10.1371/journal.pone.0124433, 2015.
46. Morishima H, Koga T, Tatsumi K, *et al*. Dose measurement, its distribution and individual external dose assessments of inhabitants in the high background radiation areas in China. J Radiat Res, **41(Suppl)** : 9–23, 2000.
47. Nair RRK, Rajan B, Akiba S, *et al*. Background radiation and cancer incidence in Kerala, India-Karunagappally cohort study. Health Phys, **96** : 55–66, 2009.
48. Tao Z, Akiba S, Zha Y, *et al*. Cancer and non-cancer mortality among inhabitants in the high background radiation area of Yangjiang, China (1979–1998). Health Phys, **102** : 173–181, 2012.
49. Wessel P, Smith WHF, Scharroo R, Luis JF, Wobbe F. Generic mapping tools : improved version released. EOS Trans AGU, **94** : 409–410, 2013.